CONF-9404162--20

UCRL-JC-118151
PREPRINT

New Infrared Solid State Laser Materials for CALIOPE

L. D. DeLoach
R. H. Page
G. D. Wilke
S. A. Payne
W. F. Krupke

This paper was prepared for submittal to the Proceedings
of the 1994 CALIOPE ITR Conference
Livermore, CA
April 26–28, 1994

August 1, 1994

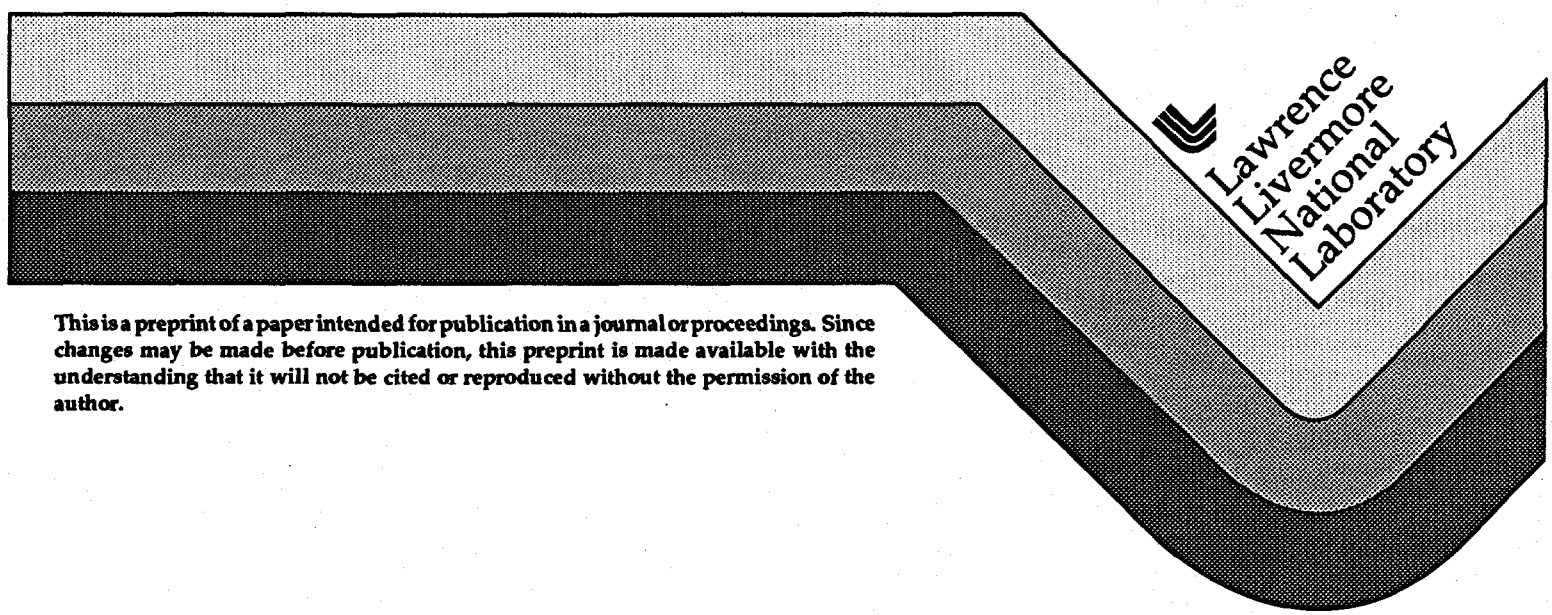

NEW INFRARED SOLID STATE LASER MATERIALS FOR CALIOPE

Laura D. DeLoach, Ralph H. Page, Gary D. Wilke, Stephen A. Payne, and William F. Krupke
Lawrence Livermore National Laboratory, Livermore, California 94551

Introduction

Tunable infrared laser light may serve as a useful means by which to detect the presence of the targeted effluents. Since optical parametric oscillators (OPOs) have proven to be a versatile method of generating coherent light from the ultraviolet to the mid-infrared, this technology is a promising choice by which to service the CALIOPE applications. In addition, since some uncertainty remains regarding the precise wavelengths and molecules that will be targeted, the deployment of OPOs retains the greatest amount of wavelength flexibility.

Another approach that we are considering is that of generating tunable infrared radiation directly with a diode-pumped solid state laser (DPSSL). One important advantage of a DPSSL is that it offers flexible pulse format modes that can be tailored to meet the needs of a particular application and target molecule. On the other hand, direct generation by a tunable DPSSL will generally be able to cover a more limited wavelength range than is possible with OPO technology. It is also noteworthy that a tunable DPSSL can serve as a means by which to seed the cavity field of an OPO.

In support of the CALIOPE objectives we are exploring the potential for laser action among a class of materials comprised of transition metal-doped zinc chalcogenide crystals (*i.e.*, ZnS, ZnSe and ZnTe). The Cr^{2+}, Co^{2+} and Ni^{2+} dopants were selected as the most favorable candidates, on the basis of their documented spectral properties in the scientific literature.[1-16] Thus far, we have characterized the absorption and emission properties of these ions in the ZnS and ZnSe crystals. The absorption spectra are used to determine the preferred wavelength at which the crystal should be pumped, while the emission spectra reveal the extent of the tuning range potentially offered by the material. In addition, measurements of the emission lifetime as a function of temperature turn out to be quite useful, since this data is suggestive of the room temperature emission yield. The diagram appearing in Figure 1 illustrates the pumping and emission processes, and also how the nonradiative decay mechanism may compete with the emission (note the k_{nrad} and k_{rad} rate constants in the figure).

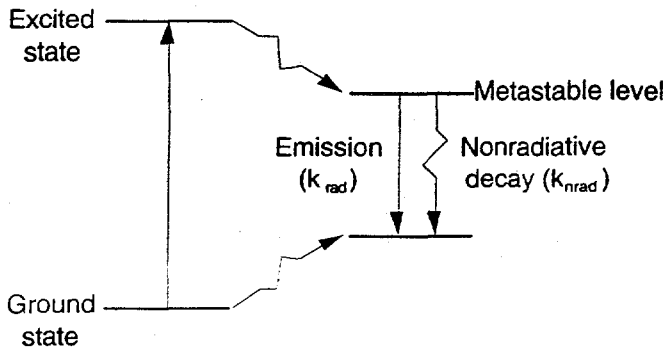

Figure 1. Absorption, emission and nonradiative processes for laser ions in crystals.

It is important to note that fundamental mechanisms impose limits on the tunability and wavelength of solid state laser materials operating in the mid-infrared. This is the case because nonradiative decay tends to become more competitive as the emission bandwidth increases, and as the wavelength of interest becomes longer (due to the initial and final states being closer together in energy). The ZnS and ZnSe hosts that we have selected, however, tend to ameliorate the detrimental impact of these effects in two ways: (a) the four-fold coordinated sites of the zinc chalcogenide crystals give rise to large dipolar fields at the metal ion site, serving to enhance the radiative rate, k_{rad}, and (b) the weakness of the crystal field splitting limits the emission bandwidth.

It is worth mentioning that the ZnS and ZnSe materials are well-developed optical crystals that are routinely employed as windows, prisms, lenses, etc.; our main contribution here is to suggest that these crystals can also be doped with transition metal ions and potentially serve as laser materials. In what follows we will cover the following topics: (a) the compatibility of transition metal doped zinc chalcogenides with laser diode pump sources, (b) the emission cross section, quantum yield, and potential tuning range, (c) thermal management issues, (d) crystalline quality, and (e) prospects for laser action. Below we display and analyze the spectroscopic parameters of six crystals, including Cr^{2+}, Co^{2+}, and Ni^{2+}, in the ZnS and ZnSe hosts.

Transition Metal Spectroscopy in ZnS and ZnSe

We have determined the room temperature absorption cross sections of the Cr^{2+}, Co^{2+} and Ni^{2+} ions in the ZnS and ZnSe hosts; these curves are plotted in Figure 2. The cross section evaluations are from unpolarized absorption spectra obtained using a Perkin Elmer Lambda 9 spectrophotometer and from the dopant ion concentrations as obtained by inductively coupled plasma-mass spectrometry (ICP-MS). The actual numbers of transition metal ions determined in the host are given as N and the sample lengths are indicated as ℓ on each of the spectra. In the case of the two Ni-doped crystals, no cross section units are being reported as a result of potential Ni-contamination during the ICP-MS

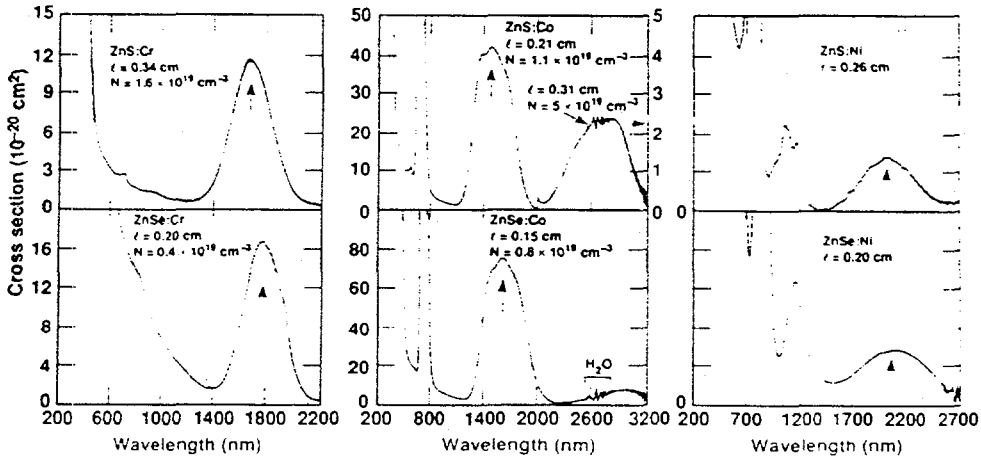

Figure 2. Absorption cross section plots of the transition metal-doped chalcogenides at room temperature. The arrows mark the potential pump bands in the 1.4 - 2.0 μm range.

analysis (this will be resolved with a new determination). Several features are indicated in the data plots of these absorption spectra. An upward-directed arrow denotes the potential IR pump band for which strained-layer InGaAs laser diodes are appropriately matched. For Co^{2+} and Ni^{2+}, the absorbance has been plotted over a spectral range which includes the water vapor lines near 2700 nm and some small scale interference is observed and indicated for these samples. The cross sections, reported in units of 10^{-20} cm^2, are generally larger for Co^{2+} than for Cr^{2+} and larger in the ZnSe host than in the ZnS.

The room temperature emission spectra have been obtained and cross section plots of the data are presented in Figure 3 for the Cr^{2+} and Co^{2+}-doped crystals of ZnS and ZnSe; the Ni^{2+} luminescence in these hosts was too weak to be observed at room temperature. The unpolarized emission spectra were collected by exciting the impurity ion with either 488 or 514 nm light from an argon laser or with 768 nm light of a Ti:sapphire laser and measuring the dispersed signal with a grating monochromator and a cooled InSb detector. The cross sections have been evaluated using the Einstein relationship which requires the lineshape function of the emission spectrum in photons/cm^{-1} or $g(\bar{\nu})$, the refractive index (n) and the radiative lifetime (τ_{rad}), for which we have employed the values recorded on the individual plots shown in Figure 3 (see discussion on lifetime determination which follows):

$$\sigma_{em} = \frac{\lambda^2 g(\bar{\nu})}{8\pi c n^2 \tau_{rad}} \qquad (1)$$

The Cr^{2+} ion is observed to have a tuning range of ~2.0-3.0 μm, whereas the Co^{2+} ion may be tunable over the range of 3.0-3.8 μm. The Cr-doped hosts have a significantly shorter radiative lifetime which leads to large cross sectional values, ~ 60-70 x 10^{-20} cm^2, compared to ~ 3 x 10^{-20} cm^2 for Co-doped hosts.

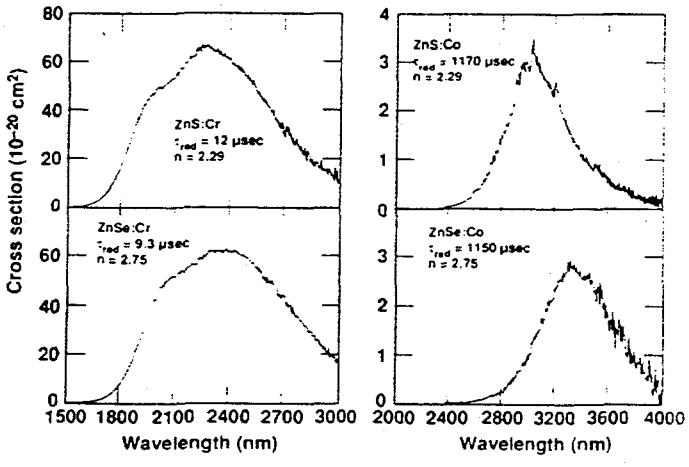

Figure 3. Room temperature emission cross section plots of the transition metal-doped chalcogenides.

Excited-state lifetimes and luminescence quantum yields

Measurements of excited-state lifetimes are of interest for completing and cross-checking the spectroscopic knowledge of the transition-metal-doped II-VI materials, and predicting the laser performance properties such as the lasing threshold, energy storage time, and the single-pass gain.

Our approach for calibrating $\sigma_{em}(\lambda)$ has been to use the emission spectral lineshape with the radiative lifetime. (This is the procedure mentioned above in the context of deriving the experimental emission cross sections.) The overall decay rate or inverse emission lifetime is the sum of the radiative and nonradiative rates:

$$k(T) = k_{rad} + k_{nrad}(T) = 1/\tau(T). \qquad (2)$$

where k_{rad} is assumed to be approximately temperature-independent. Several authors[3,12,14,15,17] have interpreted this expression in the context of the "Configuration Coordinate Model".

We can then estimate the room-temperature emission quantum yield with

$$\eta_{QY} \sim k_{rad} / (k_{rad} + k_{nrad}(RT)) = \tau(RT)/\tau(\text{low T}) \qquad (3)$$

by measuring lifetimes at room temperature and at temperatures low enough that quenching can be neglected (and the decay is assumed purely radiative).

To measure emission lifetimes, we excited the samples with the 1907 nm Raman-shifted output of a 1064 nm pulsed Nd:YAG laser. At ~10 nsec, the exciting pulsewidths were much shorter than the expected lifetimes, so the emission decay transients could be discriminated from the laser pulse. The samples were held in a vacuum cryostat and cooled with a "Displex" closed-cycle helium refrigerator, and temperatures between 15 and 300 K were used for observations. Side fluorescence was monitored through long-pass filters with photovoltaic InAs and InSb diodes, whose signals were processed with transimpedance amplifiers. Depending on details of detector gain settings, response times were as short as 1 μsec, allowing accurate lifetime measurement without deconvolution. A transient

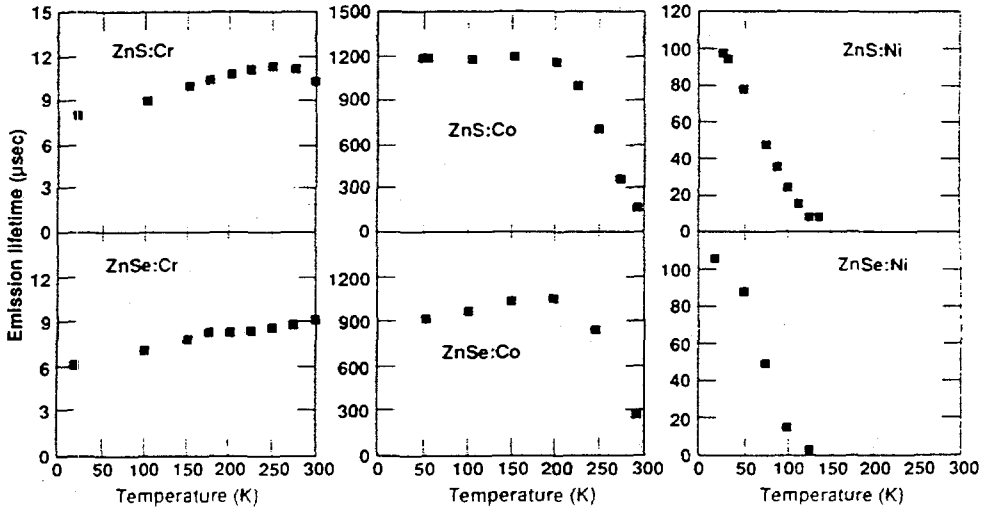

Figure 4. Lifetime plots τ(T) for the transition-metal-doped II-VI materials. At low temperatures, the decays are assumed to be purely radiative, while at higher temperatures, thermal quenching is important. From these plots, the room-temperature luminescence quantum efficiency is estimated. Chromium is seen to have a high efficiency; nickel's is negligible; and cobalt's is ~20%.

digitizer was used to average luminescence signals I(t) from typically 512 laser pulses at each temperature. Straight-line fits to plots of *ln* I(t) against time yielded luminescence decay rates $1/\tau(T)$.

Lifetime plots $\tau(T)$ are shown in Figure 4 for the six materials studied to date, including the three dopants Cr^{2+}, Co^{2+}, and Ni^{2+} in each of the hosts ZnS and ZnSe. One trend is that the lifetimes observed for each dopant are similar in magnitude and in temperature dependence when the host is changed from ZnS to ZnSe. Based on this result, we would expect rather similar behavior in ZnTe and perhaps other II-VI compounds, allowing some flexibility to tailor peak absorption and emission wavelengths, and to optimize crystal growth procedures. Another point of note is the scale of the radiative lifetimes--they span two orders of magnitude, from ~10 μsec to ~1000 μsec. This has implications for the pump schemes and output pulse formats in working lasers in that longer lifetimes allow the build-up of higher inversion density in the laser material.

The room-temperature quantum yield η_{QY} mentioned above is seen to vary dramatically between dopants. In Ni^{2+}, it is virtually zero, rendering it of little interest as a practical room-temperature laser. For Co^{2+}, there is a "knee" in the lifetime plot around 200 K, and we see that the room-temperature lifetime is ~20% of its low-temperature value, so $\eta_{QY} \sim 0.2$ for this system. In an operating laser, the stimulated emission rate can sometimes be arranged to be many times larger than the spontaneous emission rate k_{rad}, so that the energy extraction efficiency can exceed η_{QY}.

Most promising from an efficiency standpoint is the Cr^{2+} case, which also has the shortest lifetimes. The apparent slight increase with temperature of the lifetime suggests a departure from the naive model of Equation 1; the explanation of this effect is beyond the scope of this article. Recent measurements above room temperature, not displayed here, show lifetimes peaking around 300 K, and declining to 50 - 75% of their RT value at 375 K. Based on these results, we infer that $\eta_{QY} \sim 1$ for Cr^{2+} at 300K.

Laser Thresholds

Knowledge of the emission cross section, lifetime, and quantum yield allows us to predict the laser pump power threshold. The usual threshold condition, assuming fractional loss per pass of S for scatter and T for transmission through the output coupler is:

$$P_{th} = (h\nu/\sigma_{em}\tau_{em})\, A\, (S + T) \qquad (4)$$

where A is the pump size area, P_{th} is the absorbed pump power at threshold, ν is the pump frequency, and τ_{em} is the 300K emission lifetime. This equation is valid in the continuous-wave case that the pump duration τ_p is much longer than the lifetime τ_{em}. The threshold pump energy is then just

$$E_{th} = P_{th} \bullet \tau_{em} \qquad (5)$$

for $\tau_p << \tau_{em}$, and

$$E_{th} = P_{th} \bullet \tau_p \qquad (6)$$

for $\tau_p >> \tau_{em}$.

Crystal	Emission cross section σ_{em} (10^{-20} cm^2)	Emission lifetime, RT τ_{em} (μsec)	Passive loss (%/cm)	Calculated pump energy at threshold (mJ)
ZnS:Cr	66	10.4	8	0.06
ZnS:Co	3.2	190	7	0.2
ZnS:Ni	(30)	<0.1	3	>10
ZnSe:Cr	61	9.2	10	0.08
ZnSe:Co	2.8	300	25	0.3
ZnSe:Ni	(30)	<0.1	20	>20

Table I. Relevant data and calculated pump thresholds. Cavity losses, including scatter, are used with the lifetimes and emission cross sections to estimate thresholds. Here the calculations were based on 80 μsec pump pulses and 100 μm spot size.

We have estimated pump thresholds for the various materials, in the specialized case of pumping with a Co:MgF_2 laser. This system, which we intend to employ as a diode-laser surrogate, is tunable from 1700 - 2500 nm, a range that includes the desired pump wavelengths in Figure 2. Its pulsewidth τ_p ~80 μsec is well-matched to the materials' typical lifetimes, avoiding damage problems that could result from trying to deliver the requisite pump energy in a short (*e.g.*, nsec-timescale) pulse. For a spot size, we have assumed the pump and signal waves respectively have radii $\omega_p = \omega_s = 100$ μm, an achievable value for a short, stable-cavity resonator. The spot area A is taken to be $(\pi/4)(\omega_p^2 + \omega_s^2)$. Output coupling of 10% is assumed, T = 0.1. Table I displays the other input parameters needed for the threshold estimates: the cross section, lifetime, and passive loss. We assumed the use of crystals 0.5 cm long, and calculated the scatter loss by multiplying this length by the passive loss. The scatter losses have probably been overestimated, having been measured at 1064 nm, a wavelength shorter than the intended laser wavelengths.

The final column of Table I displays the predicted pump thresholds in millijoules. Where it has been assumed that only half the pump light is absorbed. Except for the nickel-doped samples, which have poor quantum yields, the thresholds in all cases are below 1 mJ, and should be easily attainable with the Co:MgF_2 test laser, which is specified to deliver up to 100 mJ per pulse.

Excited-State Absorption

An unresolved technical question is the possibility of excited-state absorption (ESA), which may counteract the desired excited-state emission. Many of the formulae used to characterize laser operation can be modified to include ESA, which we represent with the cross section σ_{ESA}, by replacing the $\sigma_{em}(\lambda)$ term with $\sigma_{em}(\lambda) - \sigma_{ESA}(\lambda)$. Clearly, if the overall, adjusted emission cross section is negative, laser action is impossible. Since it is difficult to predict the absolute magnitude of ESA, it is better to characterize it experimentally by performing a "pump-probe" experiment. When ESA is strong, pump-induced loss (optical limiting) results. We can also make informed guesses about the presence of important ESA bands on the basis of Tanabe-Sugano energy-level diagrams. In doing so, we find that in the wavelength range of interest, Cr^{2+} is free of symmetry-allowed, spin-allowed

ESA transitions. Co^{2+} and Ni^{2+}, however, are much more likely to suffer ESA losses over parts of their emission ranges.

Thermomechanical Properties of ZnS and ZnSe

The measure of a laser crystal's resistance to cracking while under a thermal load may be estimated from the thermal shock parameter, R'_T. This figure-of-merit is given as:

$$R'_T = \kappa K_{1c}(1-\upsilon)/\alpha E \qquad (4)$$

where κ is the thermal conductivity, K_{1c} is the fracture toughness, υ is Poisson's ratio, α is the thermal expansion and E is Young's modulus. For our investigation of these media as potential laser performers, we have measured or collected information on each of these thermomechanical properties for single crystal ZnS and ZnSe. Table 1 compares the R'_T values of ZnS and ZnSe with some common laser materials and a presents a separate tabulation of the thermal conductivity and dn/dT (the material's change in refractive index with temperature). We can conclude from the entries in Table 1 that both ZnS and ZnSe compare favorably to other common laser hosts. The large values of R'_T are similar to the oxide hosts and suggest that high thermal loads may be sustained in these materials without fracture. On the other hand, large positive dn/dT values may detrimentally lead to substantial thermal lensing.

Material	κ (W/m°C)	R'_T (W/√m)	dn/dT (10^{-6}/°C)
ZnS	17	7.1	+46
ZnSe	18	5.3	+70
YAG	10	4.6	+8.9
YLF	5.8	1.1	-2.0,-4.3
LG-750	0.6	0.35	-5.1
Al_2O_3 (sapphire)	28	22	+12

Table II. Thermomechanical and optical properties of ZnS and other host media

We also have measured the scatter losses at 1064 nm in the boules initially received, even though the crystal growth efforts were not anticipated to yield particularly high quality samples at this stage of our investigations. Our results are summarized above in Table I and in fact do reflect high losses and considerable variation. The Bridgman method of crystal growth from which these boules were obtained reportedly is more favorable for crystal growth of ZnS than ZnSe which appears to be consistent with the observed loss values. The preferred means of growing ZnSe crystals is by vapor growth techniques. Experience suggests that losses of <1%/cm should be attainable.

Summary

The information that we have obtained suggests that the Cr^{2+} and Co^{2+} metals may serve as useful laser ions in ZnS, ZnSe, and probably ZnTe. On the basis of our data, we have decided to ex-

clude the Ni-doped crystals from our plans to test each of these crystals for laser action. If it turns out that both Cr^{2+} and Co^{2+} are useful laser crystals, the wavelength range of 2-3.8 μm will be accessible, providing overlap with the vibrational features of numerous possible target molecules, as illustrated in Figure 5.

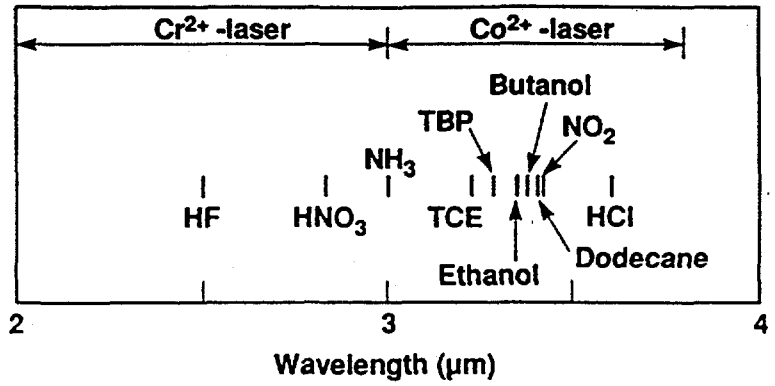

Figure 5. Spectral overlap of the anticipated tuning range of the Cr^{2+} and Co^{2+} lasers with the vibrational features of several possible target molecules.

It is enticing to realize that the success of this project may mean the availability of a broad new class of laser materials. This is true since there are many other sulfide crystals that are of potential utility, and also because numerous other first, second and third row transition metal ions can be considered as prospective laser ions. Transition metal doped chalcogenide crystals may offer substantial versatility in terms of tuning ranges, pulse formats, pump wavelengths, and other features.

Acknowledgment

This work was performed for the U.S. Department of Energy by Lawrence Livermore National Laboratory under Contract No. W-7405-ENG-48.

References

1. H. A. Weakliem, *"Optical Spectra of Ni^{2+}, Co^{2+}, and Cu^{2+} in Tetrahedral Sites in Crystals,"* J. Chem. Phys. 36, 2117-2140 (1962).
2. H.-E. Gumlich and H.-J. Schulz, *"Optical Transitions in ZnS Type Crystals Containing Cobalt,"* J. Phys. Chem. Solids 27, 187-195 (1966).
3. K. K. Dubenskii, Ya. E. Kariss, A. I. Ryskin, P. P. Feofilov, and G. I. Khilko, *"Luminescence and Absorption Associated with the Lower Terms of Co^{2+} and Ni^{2+} Ions in Single Crystals of ZnS,"* Optics and Spectroscopy 19, 353-354 (1965).
4. J. T. Vallin, G. A. Slack, S. Roberts, and A. E. Hughes, *"Infrared Absorption in Some II-VI Compounds Doped with Cr,"* Phys. Rev. B 2, 4313-4333 (1970).
5. H. Nekowski and G. Grebe, *"IR-Luminescence of ZnS:Cr,"* J. Luminesc. 1/2, 88-93 (1970).
6. W. Busse, H.-E. Gumlich, E. Neumann and D. Theis, *"On the Assignment of the Infrared Luminescence Emission of ZnS(Co),"* J. Luminesc. 3, 351-354 (1971).

7. E. M. Wray and J. W. Allen, *"Crystal Field Spectra of $3d^n$ Impurities in Zinc Selenide,"* J. Phys C: Solid State 4, 512-516 (1971).

8. G. Grebe and H.-J. Schulz, *"Luminescence of Cr^{2+} Centres and Related Optical Interactions Involving Crystal Field Levels of Chromium Ions in Zinc Sulfide,"* Z. fur Naturforsch. 29a, 1803-1819 (1974).

9. J. M. Baranowski, J. M. Noras, and J. W. Allen, *"Optical Absorption Dips caused by Vibronic Antiresonances in ZnSe:Ni and ZnSe:Ti,"* J. Phys. C: Solid State 7, 4529-4535 (1974).

10. A. P. Radlinski, *"Infrared Luminescence of Cobalt Impurities in II-VI Compounds,"* J. Luminesc. 18/19, 147-150 (1979).

11. M. Kaminska, J. M. Baranowski, S. M. Uba, and J. T. Vallin, *"Absorption and Luminescence of $Cr^{2+}(d^4)$ in II-VI Compounds,"* J. Phys. C: Solid State 12, 2197-2214 (1979).

12. A. P. Radlinski, *"Position of the Co^{2+} Level in Wide-Gap II-VI Semiconductors,"* J. Phys. C: Solid State 12, 4477-4482 (1979).

13. S. G. Bishop, P. J. Dean, P. Porteous and D. J. Robbins, *"Photoluminescence Excitation Spectroscopy of 3d Transition-Metal Ions in GaP and ZnSe,"* J. Phys. C: Solid State 13, 1331-1340 (1980).

14. R. Renz and H.-J. Schulz, *"Temperature Dependence of the Lifetime of Excited States for 3d Transition Element Centres in II-VI Crystals,"* J. Luminesc. 24/25, 721-724 (1981).

15. G. Goetz and H.-J. Schulz, "Decay of Internal Luminescence Transitions of 3d Impurities in II-VI Compounds – Recent Experiments and Refined Interpretations," J. Luminesc. 40/41, 415-416 (1988).

16. G. Goetz, H. Zimmermann and H.-J. Schulz, *"Jahn-Teller Interaction at $Cr^{2+}(d^4)$ Centres in Tetrahedrally Coordinated II-VI Lattices studied by Optical Spectroscopy,"* Z. Phys. B 91, 429-436 (1993).

17. R. Renz and H. -J. Schulz, *"The decay of infrared luminescence in II - VI compound semiconductors doped by 3d transition elements,"* J. Phys. C 16, 4917-4932 (1983).

DISCLAIMER